Dental Materials 39 (2023) 391–401

Contents lists available at ScienceDirect

Dental Materials

journal homepage: www.elsevier.com/locate/dental

Chemical, structural and cytotoxicity characterisation of experimental fluoride-doped calcium phosphates as promising remineralising materials for dental applications

Salvatore Sauro[a,*], Gianrico Spagnuolo[b], Carmela Del Giudice[b], Davino M. Andrade Neto[c], Pierre B.A. Fechine[d], Xiaohui Chen[e], Sandro Rengo[b], Xiaojing Chen[f,g,h], Victor P. Feitosa[i]

[a] Dental Biomaterials & Minimally Invasive Dentistry, Departamento de Odontologia, CEU Cardenal Herrera University, Alfara del Patriarca, Valencia, Spain
[b] Department of Neurosciences, Reproductive and Odontostomatological Sciences, University of Naples "Federico II", 80131 Naples, Italy
[c] Federal Institute of Education, Science, and Technology of Ceará, Campus Camocim, 62400-000 Camocim, CE, Brazil
[d] Grupo de Química de Materiais Avançados (GQMat) – Departamento de Química Analítica e Físico-Química, Universidade Federal do Ceará (UFC), Campus do Pici, CP 12100, Fortaleza CE 60451-970, Brazil
[e] Division of Dentistry, School of Medical Sciences, The University of Manchester, Manchester, UK
[f] Xiangya School of Stomatology and Hospital, Central South University, Changsha 410008, Hunan, China
[g] Hunan Key Laboratory of Oral Health Research, Central South University, Changsha, 410008, Hunan, China
[h] Institute of Dentistry, Dental Physical Sciences Unit, Queen Mary University of London, London, United Kingdom
[i] Research Division, Paulo Picanço School of Dentistry, 900 Joaquim Sá St., Fortaleza 60135-218, Ceará, Brazil

ARTICLE INFO

Keywords:
Crystallisation
Apatite
Fluoride
Fluor-hydroxyapatite
Biocompatibility

ABSTRACT

Objectives: This study aimed at evaluating the cytotoxicity, chemical and structural properties of experimental fluoride-doped calcium-phosphates as potential remineralising materials for dental applications.
Methods: Experimental calcium phosphates were formulated using β-tricalcium phosphate, monocalcium phosphate monohydrate, calcium hydroxide, and different concentrations of calcium/sodium fluoride salts [(5 wt%: VSG5F), (10 wt%: VSG10F), (20 wt%: VSG20F)]. A fluoride-free calcium phosphate (VSG) was used as control. Each tested material was immersed in simulated body fluid (SBF), (24 h, 15 and 30 days) to assess their ability to crystallise into apatite-like. Cumulative fluoride release was assayed up to 45 days. Moreover, each powder was placed into a medium containing human dental pulp stem cells (200 mg/mL) and their cytotoxicity was analysed using the 3-(4,5-dimethylthiazol-2-yl) − 2,5-diphenyltetrazolium bromide (MTT) assay (24 h, 48 h and 72 h incubation). These latter results were statistically analysed by ANOVA and Tukey's test ($\alpha = 0.05$).
Results: All the experimental VSG-F materials produced fluoride-containing apatite-like crystals after SBF immersion. VSG20F presented prolonged release of fluoride ions into the storage media (45d). VSG, VSG10F and VSG20F showed a significant cytotoxicity at dilution of 1:1, while at 1:5, only VSG and VSG20F demonstrated a reduction in cell viability. At lower dilutions (1:10, 1:50 and 1:100) all specimens showed no significant toxicity to hDPSCs, but an increase in cell proliferation.
Significance: The experimental fluoride-doped calcium-phosphates are biocompatible and possess a clear ability to evoke fluoride-containing apatite-like crystallisation. Hence, they may be promising remineralising materials for dental applications.

1. Introduction

Modern minimal invasive dentistry aims at preserving the natural structure of patients' teeth and keep their functional as long as possible [1]. The main strategies to accomplish such a target include early caries detection and risk assessment, adapt ideal measures for caries preventive and remineralisation of demineralised dental tissues (e.g., enamel and dentine) [2].

Lamentably, demineralisation of dental hard tissues (DDT) remains a critical issue in modern society, and it remains the main responsible for

* Correspondence to: Dental Biomaterials & Minimally Invasive Dentistry, Departamento de Odontología – Facultad de Ciencias de la Salud, Universidad CEU, Cardenal Herrera, 46115 – Alfara del Patriarca, Valencia, Spain.
E-mail address: salvatore.sauro@uch.ceu.es (S. Sauro).

https://doi.org/10.1016/j.dental.2023.03.007
Received 8 January 2023; Received in revised form 14 February 2023; Accepted 3 March 2023

erosion, dental caries and dentine hypersensitivity [3]. DDT is generated by a drop of pH, which is due to several different causes such as the intake of acidic food or drinks, the presence of gastroesophageal reflux disease or the acidogenic activity of a specific cariogenic biofilm [4]. Indeed, when the pH in the oral cavity drops below 5.5, there is an increased solubility of dental hydroxyapatite (HA), which triggers a loss of mineral such as calcium (Ca^{2+}) and phosphates (PO_4^{3-})and the formation of porosities within the enamel crystals. Such a situation causes a deeper diffusion of acids into the tooth with consequent critical demineralisation of the sub-surface of the tooth [3]. However, during such demineralisation events, the release of Ca^{2+} and PO_4^{3-} may raise the degree of saturation with respect to the enamel mineral and protect this latter from further demineralisation [5,6]. Moreover, natural remineralisation can occur through epitaxial crystallisation on Ca/P nucleation sites in enamel, whereas saliva favours super-saturation of the environment with Ca^{2+} and PO_4^{3-} [3,6,7]. Nevertheless, once the physiological equilibrium between demineralisation and remineralisation in the oral cavity is irreversibly altered, it is imperative to apply specific prophylactic agents to achieve prompt remineralisation of demineralised dental tissues. For instance, fluoride application is the most employed strategy to reduce and prevent dental demineralisation [8]. It is generally believed that it is the most effective approach to prevent caries formation thanks to two specific mechanisms: (i) alteration of the metabolism of microorganisms in the cariogenic biofilm [9]; (ii) formation of acid resistant fluorapatite [FA: $Ca_5(PO_4)_3F$] by replacing the hydroxyl groups (OH^-) with fluoride ions (F^-) within the dental hydroxycarbonate apatite [10]; such a phenomenon seems to occur especially when fluoride is present in a relatively low concentration (< 45 ppm) [11,12]. It is well known that fluoride is also used to induce the transformation of stoichiometric hydroxyapatite (HA) into a more acid resistant fluor-hydroxyapatite [FHA: $Ca_{10}(PO_4)6(OH_xF_y)$] [13,14].

Apart from fluoride, several alternative materials based on calcium phosphates [15,16] and bioactive glasses [17,18] have been advocated as suitable remineralising agents for dental hard tissues [19]. Such remineralising agents were also incorporated as ion-releasing fillers into experimental dental resin-based materials with the aim to remineralise the interface between the restoration and the dental substrate [20–23]. This target is usually achieved in vitro through the release of specific ions such as Ca^{2+} and PO_4^{3-} in specific range of pH [23,24], which may act as precursors for the deposition of apatite-like crystals within the demineralised dentine [25,26]. Moreover, such a specific remineralisation process may also protect the collagen fibrils from enzymatic degradation, so preventing the degradation of the hybrid layer [22,27]. It has also been advocated that the precipitation of crystals at the bonding interface may act as a potential physical barrier against the penetration of microorganisms, so avoiding secondary caries at the tooth-restoration interface [28–30].

Although the ability of fluoride-functionalised calcium phosphates to remineralise dental hard tissues has been already demonstrated [16], there is still a great interest in generating innovative fluoride-doped calcium phosphates as potential remineralising materials for dental applications, which may be able to react with body fluids (i.e. saliva) and convert into FA and/or FHA.

Thus, this study aimed at evaluating the ability of experimental fluoride-doped calcium-phosphates to convert into fluoride-containing apatite-like crystals. The objectives of this study were accomplished through chemical, morphological and structural characterisation of the tested materials subsequent to immersion in simulated body fluid (SBF) for different periods of storage, by means of magic angle spinning – nuclear magnetic resonance (^{19}F MAS NMR), ultra-high-resolution analytical focused ion beam scanning electron microscopy (FIB-SEM), transmission electron microscope equipped with energy dispersive X-ray spectroscopy and selected area electron diffraction (TEM-EDX-SAED), X-ray diffraction (XRD) and Fourier-transform infra-red spectroscopy (FTIR). Fluoride release, pH, and cytotoxicity of the tested materials on human dental pulp stem cells (hDPSCs) were also examined.

2. Materials and methods

2.1. Specimen preparation, pH, and fluoride release

Experimental calcium phosphates were formulated by incorporating a constant concentration of calcium hydroxide and different concentrations of fluoride salts as previously reported [31]. In brief, a 1:1 molar ratio of beta-calcium-phosphate (β-TCP: $Ca_3(PO_4)_2$) and monocalcium phosphate monohydrate (MCPM: $Ca_3(H_2PO_4)_2$) were doped with calcium hydroxide (10 wt%), calcium and sodium fluoride salts (1:1) at different concentration (5 wt%, 10 wt%, or 20 wt%). The resultant calcium phosphates doped with different concentrations of fluoride were VSG5F; VSG10F; VSG20F, while a fluoride free (VSG) calcium phosphate was also formulated and used as the control material. The simulated body fluid (SBF) employed in this study was prepared by mixing sodium chloride (NaCl: 7.996 g), sodium bicarbonate ($NaHCO_3$: 0.350 g), potassium chloride (KCl: 0.224 g), dipotassium hydrogen phosphate trihydrate ($K_2HPO_3{\cdot}3H_2O$: 0.228 g), magnesium chloride hexahydrate ($MgCl_2{\cdot}6\ H_2O$: 0.305 g), calcium chloride dihydrate ($CaCl_2{\cdot}2H_2O$: 0.368 g), sodium sulphate (Na_2SO_4: 0.071 g), and 6.057 g tris(hydroxymethyl)amino methane, $(CH_2OH)_3CNH_2$ (Tris buffer) per litre of SBF in distilled water. The pH was regulated using 1 N hydrochloric acid (HCl) as described by Kokubo et al. [32]. All chemical reagents were purchased from Merck Life Science SLU (Madrid, Spain). The experimental VSG powders (150 mg; particle size < 50 μm) were dispersed in the SBF (1.5 g/L) [14].

Five specimens were prepared for each tested powder and the pH of the solution was assessed using a pH metre (Hach Sens Ion+, SN: 705013, Hach-Langg SLU), while fluoride-release was measured using a direct potentiometry method with a liquid membrane for selective fluoride-ion electrode up to 45 days (45d). Four standard fluoride-containing solutions (1 $mg.L^{-1}$, 5 $mg.L^{-1}$, 10 $mg.L^{-1}$ and 100 $mg.L^{-1}$) were used for calibration of the Ion (Fluoride)-selective electrode (ISE, NT-F-MD019), using the reference electrode Ag/AgCl (SK-402–75B-CR) by XS 80 +DHS (XS Instruments, Italy) [13]. After each reading, the electrode was washed with osmosis water. Fluoride release data were expressed in (mg/L) and analysed statistically by Kruskal-Wallis and Bonferroni tests, with a significance level of 5 %.

2.2. FTIR vibrational spectroscopy

Each experimental VSG powder was dispersed in the SBF as aforementioned and agitated at a rate of 60 rpm in an orbital shaker for 5 min. Subsequently, the specimens were left undisturbed at 37 °C in SBF, which was replaced every 7 days. Each powder was filtered through medium porosity filter papers after different periods of immersion in SBF (24 h, 15d and 30d) and subsequently dried at 40 °C for 24 h. These were submitted to vibrational analysis in triplicate and the spectra were recorded in the range 3000–500 cm^{-1} with 32 scans at 4 cm^{-1} resolution using the Spectrum Two FT-IR Spectrometer equipped with attenuated total reflection (ATR) device (Perkin Elmer, Madrid, Spain). The peaks were analysed subsequent to baseline subtraction and normalisation using the Spectrum 10™ software (Perkin Elmer) in order to identify the most characteristic inorganic compounds in the specimens.

2.3. X-ray diffraction (XRD)

After the FTIR analysis, the specimens were submitted to XRD using the X-ray powder diffractometer X'Pert MPD (PANalytical, Westborough, USA) equipped with CuKα tube (λ = 1.5418 nm), 40 kV of voltage and a 30 mA current in a range of scanning 2θ = 20–80°. The diffraction patterns were obtained by using Bragg–Brentano geometry in continuous mode with speed of 0.5°/min and step size of 0.02° (2θ). The Rietveld structure refinement was used for interpreting and analysing the diffraction data using the software DBWS Tools [33]. Using

this type of refinement, it was possible to obtain important information regarding molar fraction and size of apatite particles [34,35]. The progress, as well as the quality of the refinement was demonstrated in terms of weighted factor RWP (percentage of error obtained) and S factor (goodness of fit); such values for the refinement of all specimens revealed a successful calculation [34,35]. The size (D) of the crystals was also calculated from the refinement data using the following Scherrer equation

$$D = \frac{K\lambda}{\beta\cos\theta}$$

Where K is a constant, λ is the wavelength of the X-ray, θ is a Bragg diffraction angle and β is the full width at half-maximum (FWHM). It is important to mention that the instrumental FWHM was calculated though the XRD measurement using LaB_6 NIST standard sample and subtracted from FWHM of the sample.

2.4. ^{19}F MAS NMR

The experimental calcium phosphates were also investigated using ^{19}F MAS NMR on a Bruker Avance III 400 (400 MHz, 9.4 Tesla) NMR spectroscopic device to identify the presence of fluorapatite (FA) and/or fluor-hydroxyapatite (FHA) subsequent to 30 days of storage in SBF. Spectra were recorded using a 4 mm wide bore triple resonance Bruker probe spinning at 10,560 Hz. The delay time used was 1.0 s. Spectrum of a synthetic fluorapatite was collected and used as comparison [13]. The ^{19}F chemical shift was referenced to an external standard of C_6F_6 (hexafluorobenzene) primary standard [14].

2.5. Chemical and morphological characterisation (FIB-SEM/TEM-EDX-SAED)

Similar to the previous tests performed in this study, each experimental VSG powder, along with hydroxyapatite (99.8%, HAP, Merck Life Science SLU, Madrid, Spain), was analysed at baseline (24 h) and after 4 weeks of storage in SBF periods. The specimens were suspended in ethanol and the nano-suspensions were deposited on carbon-coated copper grid and analysed using the transmission electron microscope (TEM, Tecnai G2 F30, FEI, Eindhoven, The Netherlands). Moreover, the specimens were also examined through selected area electron diffraction (SAED) and energy-dispersive x-ray spectroscopy analyses (EDX - kV: 200.00 Azimuth: 45.00 Elevation: 35.00 AmpT: 51.2). During the EDX analysis, the specimens were assessed in six different areas in order to calculate the Ca/P ratio of the crystals [36]. Further specimens were mounted on aluminium stubs with carbon cement and gold-sputter-coated to be subsequently analysed using a ultra-high-resolution analytical focused ion beam scanning electron microscopy (FIB-SEM, Thermo Scientific Scios 2 DualBeam, Waltham, Massachusetts, USA) in secondary electron mode. The FIB-SEM was equipped with an energy dispersion-type x-ray spectroscope (EDX), which was used at 20 kV to analyse the presence of fluoride in the tested materials.

2.6. Cell viability and proliferation

Human Dental Pulp Stem Cells (hDPSCs) were purchased from Lonza (PT-5025, Swiss, Basel, Switzerland) and used in this study. These were cultured following manufacturer' instructions and maintained in a medium containing DPSC (BulletKit™ Medium, PT-3005, Lonza, Walkersville, USA) in an incubator at the temperature of 37 °C and 5 % CO_2.

Each powder was immersed in SBF for 24 h and then diluted in DPSC medium at the concentration of 200 mg/mL, in accordance with the ISO/EN 10993–12 [37]. After incubation at 37 °C for 24 h at 5 % CO_2, the eluate was recovered and sterilised using a 0.2-mm filter (Merck Millipore, Tullagreen, Carrigtwohill, Co. Cork, Ireland). Serial dilutions of powder extracts were prepared (1:1 (non-diluted), 1:5, 1:10, 1:50, 1:100) in DPSCs medium.

The cytotoxicity of the powders on DPSCs was evaluated using the MTT [3-(4,5- dimethylthiazol-2-yl) − 2,5-diphenyltetrazolium bromide] assay, according to the manufacturer's instructions (Sigma-Aldrich, M5655 St. Louis, USA). The cells were placed into a 96-well at an initial density of 5×10^3 cells/well; after 24 h, the extracts were added to the 96-wells and hDPSCs were incubated for 24, 48, and 72 h. At each time point, the medium of the controls and eluates were eliminated by each well and the MTT solution was added and incubated for 4 h at 37 °C and 5 % CO_2. At the end of the incubation period, the medium was removed and the converted dye was solubilised with acidic isopropanol (0.04–0.1 N HCl in absolute isopropanol). Absorbance was measured at 570 nm using a microplate reader (Tecan, Grödic, Austria). Cells cultured on tissue culture plates with DPSCs medium were used as a control (CTL). The results were obtained in four replicates from 4 separate experiments for each test. The results were presented as mean (± SD) and the statistical analysis of the data was performed by means of an analysis of variance (ANOVA) followed by a Tukey's test for multiple comparison ($\alpha = 0.05$) [37,38].

3. Results

3.1. pH and fluoride release

The influence of the tested materials with increasing fluoride content on pH of the storage media over a period of 45 days can be seen in Table 1. It was observed that the pH of the storage media containing the experimental fluoride-doped calcium phosphates presented higher values compared to the fluoride-free VSG. In particular, VSG20F showed the highest values (mean pH:7.6), while the fluoride-free VSG had a pH of 6.4; however, this latter increased to 7.0 after 45 days of storage. Conversely, all the tested fluoride-containing materials presented no drastic change of the pH over time. In terms of fluoride ions release (mg/L), the results can be found in Table 2. It was interesting to observe that VSG5F showed no significant ($p < 0.05$) release of fluoride compared to the fluoride-free VSG up to 24 h. Moreover, VSG5F showed no significant variation of fluoride over time ($p > 0.05$), except at day 45. Contrariwise, VSG10F presented significantly higher ($p < 0.05$) release of fluoride ions compared to VSG5F at all periods of time, with the cumulative values that significantly increased over time ($p < 0.05$). On the other hand, VSG20F presented the greatest ($p < 0.05$) release of fluoride ions compared to all the tested materials. In particular, this latter material showed a significant increase in fluoride released at day 1, day 30 and day 45 ($p < 0.05$); 99.15 mg/L of cumulative fluoride was detected for the VSG20F at day 45 of SBF storage.

3.2. FTIR-ATR vibrational spectroscopy

In Fig. 1 it is possible to observe the results obtained during the FTIR vibrational analysis. The commercial hydroxyapatite (HA) presented characteristic bands corresponding to the PO_4 group at 1092 cm^{-1} and 1022 cm^{-1}, which are associated with the stretching vibrations out of plane $(\nu_3)_{so}$ of P-O, whereas the weak (w) band at 962 cm^{-1} was related to the symmetrical stretching vibration $(\nu_3)_{ss}$ of O–P–O. The strong bending vibrations $(\nu_4)_b$ of O–P–O can be observed at 560 $cm^{-1}$and 602 cm^{-1} [39,40]. Furthermore, the commercial β-TCP showed bands at

Table 1
Influence of the tested materials with increasing fluoride content on pH of the storage media over a period of 45 days.

	24 h	7 days	15 days	45 days
VSG	6.4 ± 0.1	6.8 ± 0.1	6.9 ± 0.1	7.0 ± 0.1
VSG5F	7.2 ± 0.1	7.3 ± 0.1	7.2 ± 0.1	7.4 ± 0.1
VSG10F	7.3 ± 0.1	7.4 ± 0.1	7.5 ± 0.1	7.5 ± 0.1
VSG20F	7.6 ± 0.1	7.6 ± 0.1	7.5 ± 0.1	7.5 ± 0.1

Table 2
Fluoride release (mg/L) from the tested materials over a period of 45 days.

Day	0: VSG	5 %: VSG5F	10: VSG10F	20: VSG20F
0	$2.2{\cdot}10^{-2} \pm 2.61{\cdot}10^{-3}$ A	$0.13 \pm 3.37{\cdot}10^{-2}$B	13.03 ± 0.66 C	41.13 ± 4.22D
1	$6.3{\cdot}10^{-3} \pm 3.93{\cdot}10^{-3}$ A*	$4.50{\cdot}10^{-3} \pm 8.37{\cdot}10^{-4}$A*	10.86 ± 0.55B*	40.73 ± 2.88 C
4	$1.7{\cdot}10^{-4} \pm 4.08{\cdot}10^{-4}$ A*	$5.17{\cdot}10^{-3} \pm 1.17{\cdot}10^{-3}$B	2.73 ± 0.097 C*	34.25 ± 2.73D*
7	$3.5{\cdot}10^{-3} \pm 1.64{\cdot}10^{-4}$ A*	$5.67{\cdot}10^{-3} \pm 1.21{\cdot}10^{-3}$A	6.10 ± 0.22B*	35.93 ± 3.09 C
15	$1.0{\cdot}10^{-3} \pm 2.61{\cdot}10$ A*	$6.33{\cdot}10^{-3} \pm 5.16{\cdot}10^{-4}$B	4.82 ± 0.77 C*	36.07 ± 2.30D
30	$8.2{\cdot}10^{-3} \pm 7.53{\cdot}10^{-4}$ A*	$6.33{\cdot}10^{-3} \pm 5.17{\cdot}10^{-4}$B	11.52 ± 0.08 C*	55.97 ± 0.15D*
45	$3.1{\cdot}10^{-2} \pm 1.34{\cdot}10^{-2}$ A*	$7.05{\cdot}10^{-2} \pm 4.32{\cdot}10^{-3}$B*	20.40 ± 0.14 C*	99.15 ± 0.68D*

Same letter indicates no significant difference in the values in rows.
The symbol* indicates a significant difference in the values in columns.

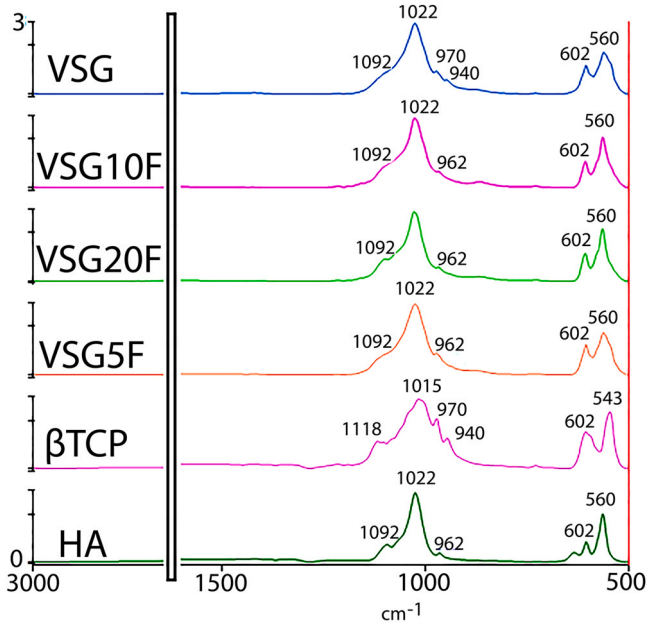

Fig. 1. FTIR-ATR spectra of the tested materials after SFB storage. Please note the characteristic peaks of commercial HA and β-TCP analysed at baseline. VSG at 4 weeks of SBF storage is still characterised by the presence of β-TCP, while VSG5F, VSG10F and VSG20F at 2 weeks of SBF storage present already a spectrum comparable to that of pure HA.

940 cm^{-1}, 970 cm^{-1}, 1015 cm^{-1}, 1118 cm^{-1} characteristic of PO_4 groups, while further PO stretch vibrations were observed at 543 $cm^{-1}$and 602 cm^{-1} [39,41]. VSG5F, VSG10F and VSG20F were characterised by a spectrum totally comparable to that of HA just after 15 days of storage in SBF. Conversely, the fluoride-free VSG presented incomplete conversion into HA, but the presence of characteristic peaks of β-TCP even after 30 days of storage in SBF.

3.3. X-ray diffraction (XRD)

The results obtained during the qualitative and quantitative XRD analysis of the tested materials are depicted in Fig. 2 and Table 3, respectively. In particular, it was possible to observe that all the experimental materials analysed after 24 h of SBF storage showed a predominant existence of β-TCP. However, VSG5F, VSG10F and VSG20F were already characterised by an early signal of HA formation, along with the presence of CaF_2. While, in the fluoride-free VSG, slight apatite-like and brushite ($CaHPO_4{\cdot}2\,H_2O$) phases were detected, along with a strong presence of β-TCP (Fig. 2A and Table 3). Structural refinement demonstrated that VSG5F had the higher molar fraction of HA with respect to β-TCP, after immersion in SBF for 24 h (Table 3).

The specimens of VSG5F, VSG10F and VSG20F immersed for 15 days in SBF were characterised by a predominant presence of HA, but with the presence of residual β-TCP. Again at 15 days of SBF storage, all the experimental materials doped with fluoride presented a clear presence of CaF_2, especially in the specimens VSG20F and VSG10F. Conversely, the fluoride-free VSG showed the presence an important presence of β-TCP, with slight precipitation of HA, and no sign of brushite anymore (Fig. 2B and Table 3).

The situation for the fluoride-free VSG remained unaffected after 30 d of SBF storage, as it was still characterised by a prominent presence of β-TCP, although an increased presence of HA (%molar) was detected. Conversely, in accordance with the reported data ICDD/PDF-16742, it was observed that the relative intensities of the diffraction peaks (i.e. crystallinity, 2θ = 30.2°(0 0 2)) became greater with the fluoride-doped powders (VSG5F > VSG10F > VSG20F); no β-TCP (% molar con.) was detected in VSG5F, VSG10F, VSG20F. It was evident in VSG20F the greatest presence of CaF_2 (Fig. 2C and Table 3).

Moreover, after 30 d of SBF storage of the tested materials containing increased amount of fluoride within their compositions, the diffraction peaks of HA in the region of 30–35º became sharper, as well as the % molar HA. It was also interesting to see the relativity intensity of the peak in 2θ at 32.3º (112) that became greater than the peak in 2θ at 33.0º (030).

Structure refinement was performed in order to calculate crystallite size and to have a good fit between the diffractogram calculated (Y-calc) and observed (Y-obs) (Fig. 2). The results of the crystal size measurement of HA calculated by means of XRD can be found in Table 3. The size of the crystal for the HA produced by VSG was very small (10.4 ± 0.3 nm), which presented no great increase over time, even after 30 d in SBF (11.3 ± 0.3). Conversely, all the fluoride doped calcium phosphates tested in this study showed an evident increase in the crystal size both after 15 and 30 ds of SBF storage. VSG5F showed the smallest crystal size at all time periods when compared to the 3 experimental fluoride-doped VSG materials tested in this study. Thus, the higher the concentration of fluoride within the composition of our experimental calcium phosphates, the greater the ability of HA crystals to increase in dimension. Conversely, the higher the concentration of fluoride, the greater the presence of CaF_2.

3.4. ^{19}F MAS NMR

The results obtained during the 19 F MAS NMR analysis are shown in Fig. 3. ^{19}F NMR spectrum of VSG5F and VSG10F after 30 days of storage in SBF revealed overlapping signals of chemical shift at − 102 ppm and a small wide shoulder at around − 106.3 ppm indicating the presence of fluorapatite-like phase and CaF_2 respectively. With an increasing amount of fluoride in VSG20F, the chemical shift at − 102 ppm became less pronounce and in contrast the peak at − 106.3 ppm became clearly and dominating. It is interesting to note that a split peak with peak chemical shifts approximately at − 102 ppm and − 111 ppm and a peak at − 128 ppm were noticed for VSG specimens, indicating a lack of conversion into apatite even after 30 days of immersion in SBF.

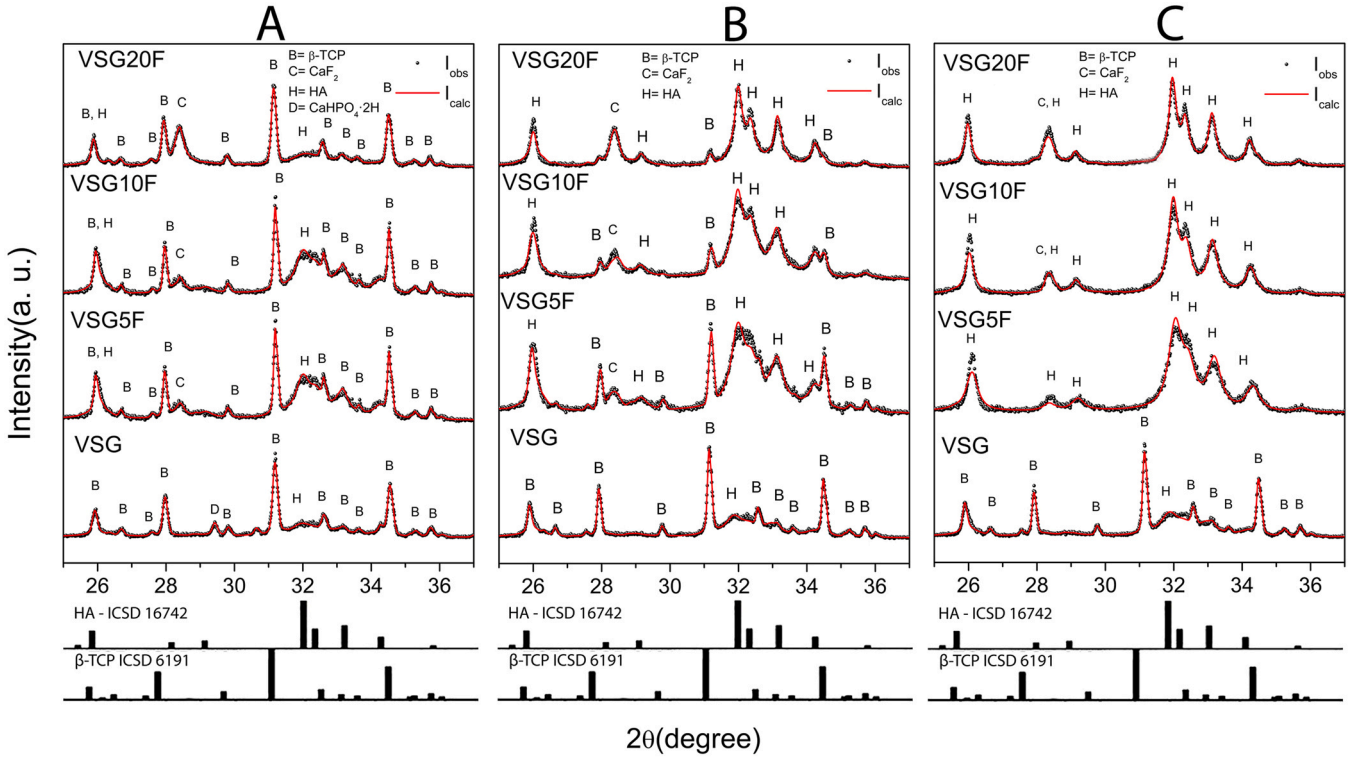

Fig. 2. XRD patterns of the tested materials after SFB storage. A. All the tested materials analysed after 24 h of SBF showed the presence of β-TCP. However, the VSG powders doped with fluoride showed the presence of CaF_2 and the presence of HA. The fluoride-free VSG showed an important presence of β-TCP and brushite ($CaHPO_4{\cdot}H_2O$) (D), but a very little signal of HA precipitation. B. At 15 days of storage in SBF, VSG20F and VSG10F showed a clear presence of HA, although there is some residual β-TCP. CaF_2 is present in the VSG powders doped with fluoride. The fluoride-free VSG is still mainly characterised by the present of β-TCP and a slight presence of HA precipitation, but with no more $CaHPO_4{\cdot}H_2O$. C. After 30 days of storage in SBF all the VSG-F powders transformed into HA. VSG20F is characterised by the highest presence of CaF_2, although all of the VSG-F powders are characterised by the presence of CaF_2,. The fluoride-free VSG is still mainly characterised by the present of β-TCP, with some HA precipitation.

Table 3
Results of the molar fraction and crystals size measurement of apatite calculated by means of XRD.

% Molar β-TCP		% Molar HA	HA Crystal Size (nm)
VSG-24 h	59.8 ± 1.3	12.9 ± 0.7	10.4 ± 0.3
VSG-15d	76.7 ± 1.3	23.3 ± 0.8	11.3 ± 0.2
VSG-30d	76.7 ± 1.32	23.3 ± 0.6	11.3 ± 0.3
VSG5F-24 h	46.4 ± 1.81	26.8 ± 0.4	14.1 ± 0.4
VSG5F-15d	45.5 ± 0.42	33.3 ± 3.6	16.5 ± 0.3
VSG5F-30d	X	100 ± 0.0	18.6 ± 0.4
VSG10F-24 h	46.8 ± 1.1	14.4 ± 0.6	13.9 ± 0.7
VSG10F-15d	13.2 ± 5.8	47.4 ± 0.7	23.8 ± 0.6
VSG10F-30d	X	84.2 ± 0.4	25.4 ± 0.9
VSG20F-24 h	33.5 ± 0.7	7.07 ± 0.6	8.4 ± 0.1
VSG20F-15d	2.0 ± 18.73	29.4 ± 0.4	36.5 ± 1.4
VSG20F-30d	X	38.6 ± 0.4	38.9 ± 1.4

Please note that excluding the VSG, all the fluoride-doped VSG present an increase in the dimension of the HA crystals. Furthermore, note that percentages reported in this table do not sum 100% since the molar fraction of CaF2 (or brushite for fluoride-free samples) are not shown.

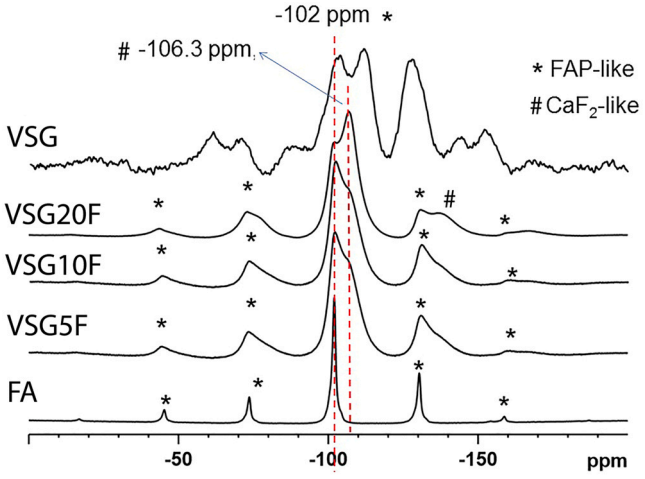

Fig. 3. ^{19}F MAS NMR spectra of the tested materials after 30 days of SFB storage. Asterisks mark spinning side bands of fluorapatite (FAP)-like, while hashtags mark spinning side bands of calcium fluoride (CaF_2)-like precipitant.

3.5. Chemical and morphological characterisation (FIB-SEM/TEM-EDX-SAED)

The most relevant morphological features observed with the tested materials after different periods of storage in SBF are illustrated in Fig. 4 (FIB-SEM) and Fig. 5 (TEM). It was interesting to observe through FIB-SEM that the fluoride-free VSG after 30 d of immersion in SBF was characterised by crystals with an irregular globular morphology (Fig. 4A) and no fluoride was detected during EDX analysis (Fig. 4A1). Conversely, all the experimental fluoride-doped calcium phosphates showed a evident presence of needle-like apatite crystals, especially in those VSG powders containing 5 wt% and 10 wt% of fluoride (Fig. 4B). In all the fluoride-doped VSG tested powders, fluoride was detected during EDX analysis (Fig. 4B1).

The TEM analysis performed after 24 h of SBF immersion showed that the VSG (fluoride-free) was characterised by few small and irregular crystallites (Figs. 5A and 5a). Moreover, such particles presented

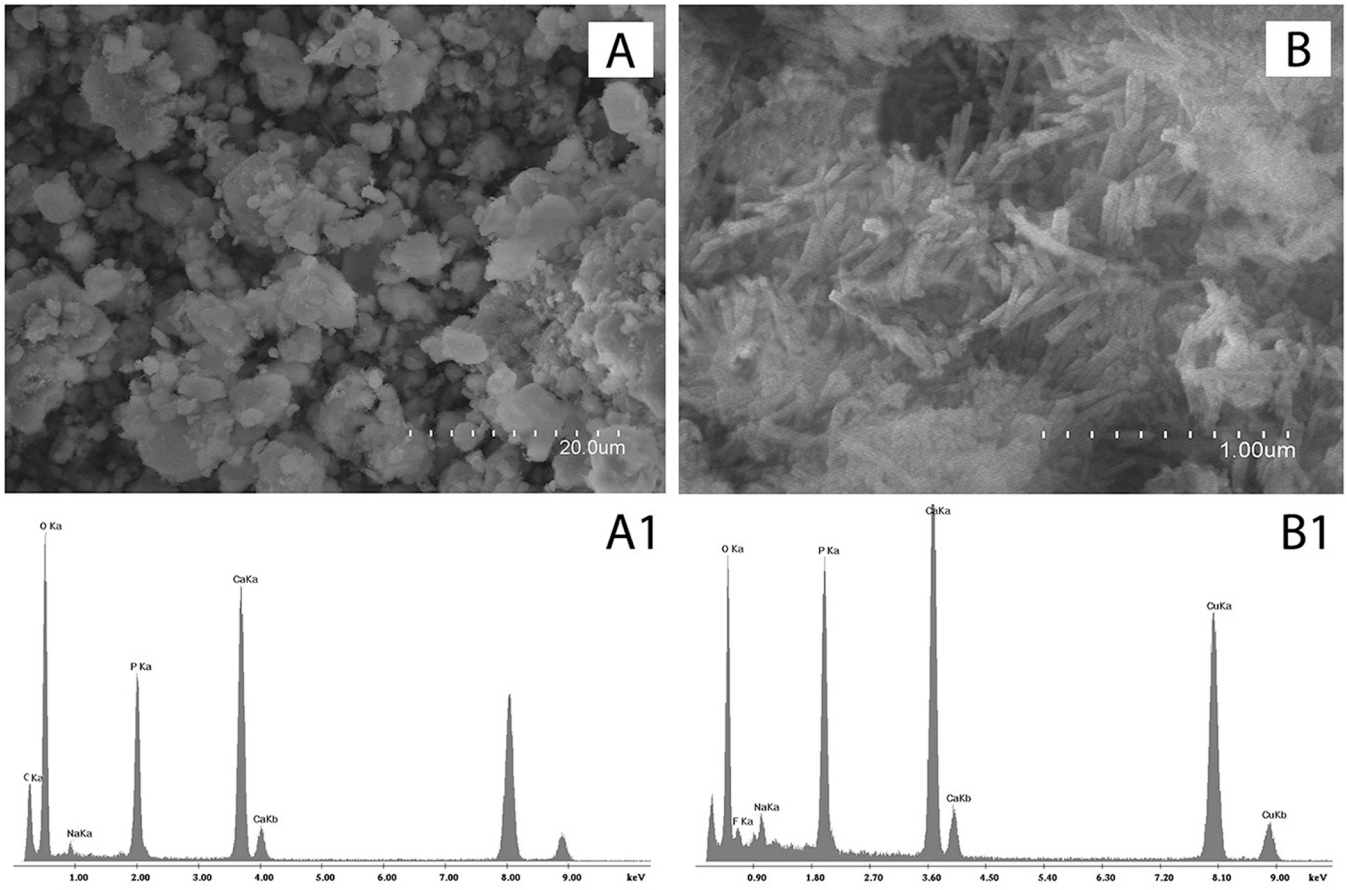

Fig. 4. FIB-SEM micrographs and EDX of the tested materials after SBF storage. A: Representative FIB-SEM micrograph of VSG (fluoride-free) after 30 days of SBF immersion showing irregular and globular particles, with no presence of fluoride in the EDX spectra (A1). B**:** Representative FIB-SEM micrograph of VSG5F after 30 days of SBF immersion showing a predominant presence of needle-like crystals, with the presence of fluoride in the EDX spectra (B1).

sign of crystallinity at higher magnification (Fig. 5a) and during SAED analysis (Fig. 5a1). However, after 30 days of storage in SBF, VSG produced a very slight increase in the number of crystals (Fig. 5B); these also appeared with a more regular rod-like morphology (Fig. 5B) compared to those observed at 24 h of SBF storage, and they were often characterised by a clear crystalline phase (Fig. 5b and 5b1). All the VSG powders doped with fluoride presented many more crystals, with increase dimension and a more regular morphology compared to those observed in the fluoride-free VSG (Fig. 5C). However, at higher magnification (Fig. 5c) and through SAED (Figure 5c1), such crystals appeared characterised by a clear crystalline phase.

After 30 d of SBF immersion all the tested calcium phosphates doped with fluoride showed an evident conversion in to large rod-like crystals (Fig. 5D), with well-well-defined crystallinity (Fig. 5c and Fig. 5 c1).

The Ca/P ratio of the tested materials before and after SBF storage can be found in Table 4. It was possible to see that the commercial HA (Merk), used as the control, had a Ca/P ratio of 1.68 ± 0.15 after 24 h of SBF immersion and 1.70 ± 0.11 after 30 d of storage in SBF. The fluoride-free VSG had a Ca/P very much different from that of HA both at 24 h (1.26 ± 0.04) and after 30 d of SBF storage (1.34 ± 0.07). The situation was slightly different for the fluoride-doped VSG5F; although it had a Ca/P of 1.34 ± 0.05 at 24 h (octacalcium phosphate - OCP), after 30 d of SBF immersion it presented a ratio (1.68 ± 0.03) quite comparable to that of the HA. Conversely, VSG10F and VSG20F presented a Ca/P ratio of 1.52 ± 0.09 and 1.54 ± 0.05 (calcium-deficient hydroxyapatite), respectively. These latter values were much higher than those obtained with VSG and VSG5F at 24 h. Moreover, after 30 days of storage in SBF, VSG10F and VSG20F presented a Ca/P ratio of 1.69 ± 0.04 and 1.74 ± 0.02, respectively. These values were comparable to that of HA (1.70 ± 0.11) after 30 d of SBF immersion.

3.6. Cell viability and proliferation

The powder extracts had different effects on hDPSCs viability. VSG and VSG20F showed the greatest ($p < 0.05$) toxic effect, at 1:1 and 1:5 dilutions. Compared to the control, VSG and VSG20F 1:1 dilution caused a statistically significant decrease in cell viability of 56 % ($p = 0.0016$) and 60 % ($p = 0.0005$) respectively after 24 h, in comparison to VSG5F and VSG10F that showed reduction of 25 % and 42 % ($p = 0.0291$) at the same time of evaluation (Fig. 6A). Nonetheless, VSG showed the major toxicity after 48 h at 1:1 dilution, with a reduction of cell viability of 59.2 % ($p = 0.0008$) (Fig. 6A). Moreover, a similar trend was measured at the dilution 1:5 (Fig. 6B). Indeed, a decline of 28.1% in cell viability for VSG was observed. In contrast, there was a decrease in viability with VSG20F of 29 % after 24 h and 34 % after 72 h. Furthermore, the data showed that 1:10 is the first dilution in which VSG had no decrease on cell viability at each time point, whilst VSG20F was the only one with decrease in cell viability (11 % at 24 h and 18 % at 48 h) (Fig. 6C). At dilutions of 1:50 and 1:100, no reduction in cell proliferation was shown in all 4 groups (Figs. 6D and 6E).

4. Discussion

One of the most critical aspects in the remineralisation of dental hard tissues is the dissolution rate of newly-formed hydroxyapatite (HA) in the oral environment, especially when important pH changes due to dietary acids intake and/or cariogenic biofilm formation arise [3–5]. This is the reason why any modifications that would offer to HA

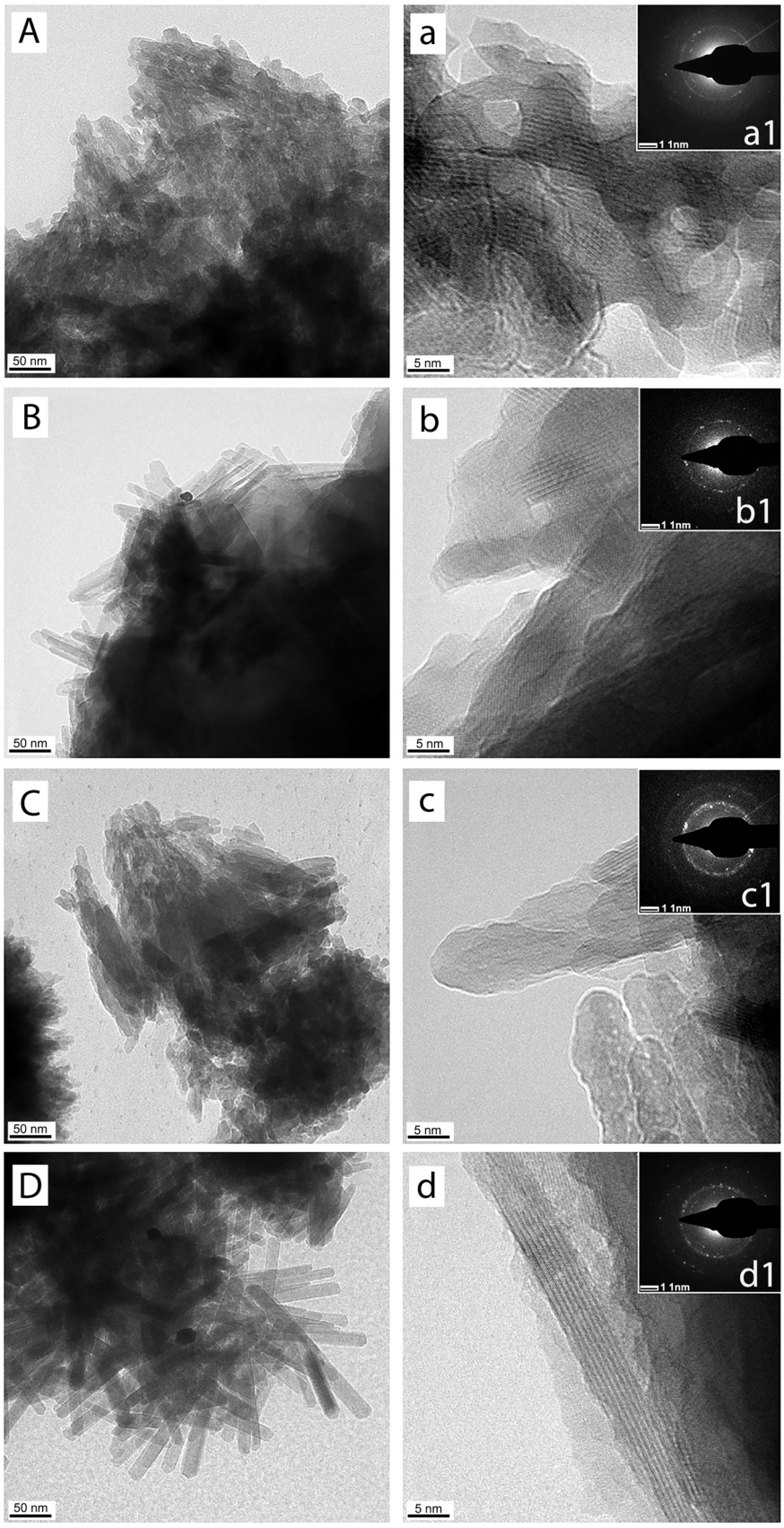

Fig. 5. TEM micrographs and Selected Area Electron Diffraction (SAED) of the tested materials after SBF storage. A: Representative TEM micrograph of VSG (fluoride-free) after 24 h of SBF immersion showing very few small and irregular crystallites (a). At higher magnification (a) and through SAED (a1), the crystallinity of such experimental material was only rarely observed. B: The VSG (fluoride-free) after 30 days of SBF immersion was characterised by the presence of some crystals with a more regular rod-like morphology (b) compared to those observed at 24 h SBF storage. Also in this case it is possible to see the crystallinity of the such experimental material (b1). C: Representative TEM micrograph of VSG10F after 24 h of SBF immersion showing several irregular crystallites (c). At higher magnification (c) and through SAED (c1), it is possible to see the crystallinity of the such experimental material. D**:** Representative TEM micrograph of VSG5F after 30 days of SBF immersion showing that the materials was fully characterised by crystallites, with a very regular rod-like morphology. At higher magnification (c) and through SAED (c1), it is possible to see the crystallinity that characterised all the tested fluoride-containing materials.

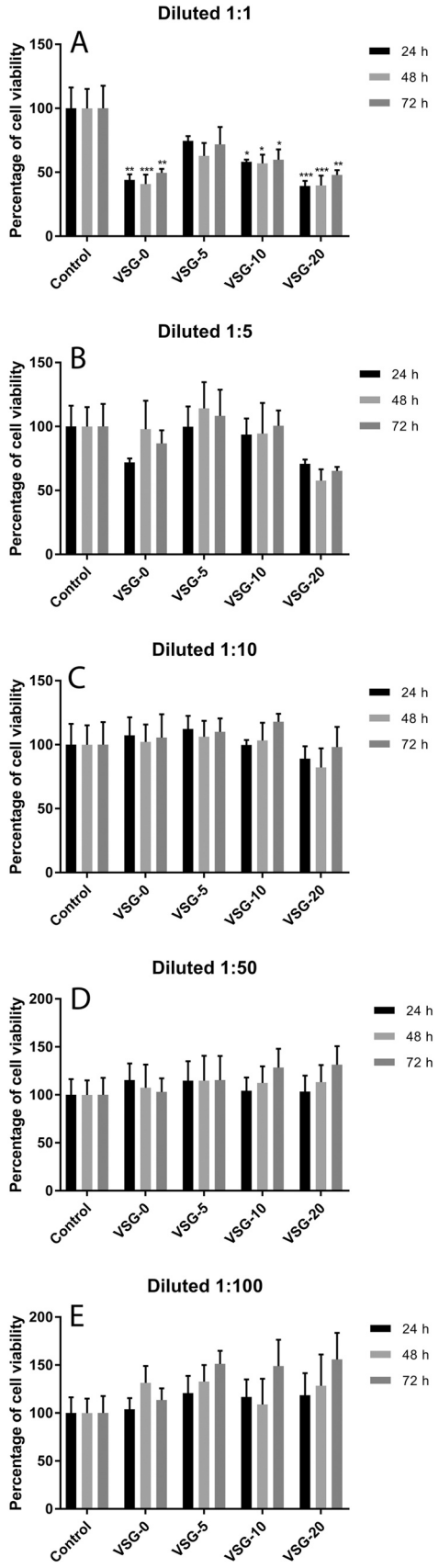

Fig. 6. MTT assay performed on human pulp dental stem cells (hPDSCs) treated with VSG, VSG5F, VSG10F, VSG20F eluates at different dilutions. Data shown are the mean (± SD) of four replicates. significant differences compared to the control are marked as * $p < 0.05$, ** $p < 0.01$, and ***$p < 0.001$, respectively.

greater chemical stability can be considered an advantage for dental remineralisation [42]. For instance, in presence of specific concentrations of fluoride, it is possible to obtain the formation of a more thermodynamically stable fluorapatite (FHA) [43]. It is important to anticipate that fluoride incorporation in a calcium phosphates to obtain fluor-hydroxyapatite and fluorapatite was previously investigated by several authors [16,43], but the novelty of the fluoride-doped calcium phosphates tested in the current study can be attributed to their simple method of production and to their ability to precipitate quite quickly in form of apatite-like crystals when immersed in simulated body fluids, and subsequently convert into fluoride-containing apatite over a period of 30 days of immersion in SBF [31]. It is well know that beta-calcium-phosphate (β-TCP: $Ca_3(PO_4)_2$) and monocalcium phosphate monohydrate (MCPM: $Ca_3(H_2PO_4)_2$) when immersed in water generate an acidic pH and precipitate as di-calcium-phosphates such as brushite ($CaHPO_4{\cdot}2H_4O$), or in some specific condition, as monetite ($CaHPO_4$) [44,45]. The fluoride-free VSG used in this study is made of equivalent amount of β-TCP and MCPM, but with the presence of an alkalinising agent (calcium hydroxide: $Ca(OH)_2$), which maintains the pH of the immersion solution above 5.5, so reducing the precipitation of brushite, but favouring that of OCT for VSG5F and calcium-deficient apatite-like crystals for VSG10F and VSG20F (Table 4), with different amount of remaining unreacted β-TCP (Fig. 2). The reason to avoid the precipitation brushite was because it is stable once precipitated and it can only convert into hydroxyapatite when immersed for a specific period of time in an alkaline solution (pH > 10), super-saturated with calcium ions (Ca^{2+}); this transformation is used in bio-engineering for the biomineralisation of bone tissues [46]. Nevertheless, although the alkalinising agent in VSG allowed only a little precipitation of brushite during the first 24 h of immersion in SBF (Fig. 2A), there was no benefit on the ability of VSG to convert into apatite. Indeed, it has been reported that self-setting cements consist of dicalcium phosphate anhydrous (DCPA), dicalcium phosphate dihydrate (DCPD), tricalcium phosphate and $Ca(OH)_2$ may convert into hydroxyapatite only if mixed in an high pH solution (pH > 11) [47]. Moreover, $Ca(OH)_2$ can be used as precursor to encourage the formation of carbonate apatite (CHA) [48].

In our pilot studies, fluoride-doped experimental calcium-phosphates were also formulated without the presence of any alkalinisation agent and there was an important precipitation of brushite as soon as they were immersed in SBF. Conversely, its presence in the tested fluoride-doped experimental calcium-phosphates had a crucial role in preventing the precipitation of brushite, but favouring that of apatite-like compounds.

As already mentioned in the introduction, the main aim of this was to evaluate the ability of tailored experimental calcium-phosphates doped with different concentrations of fluoride salts to crystallise into fluoride-containing apatite-like crystals over a period of immersion in SBF for 30 days. Several significant results were obtained during the chemical, morphological and structural characterisation. For instance, during the test performed through FTIR (Fig. 1) and XRD (Fig. 2C and Table 3),the control fluoride-free powder (VSG) was unable to convert completely into apatite-like crystals; it was characterised by an evident presence of β-TCP even after 30 days of storage in SBF. Moreover, both during FIB-SEM (Fig. 4A) and TEM (Fig. 5B) ultramorphology analysis, the fluoride-free VSG showed only very few small and irregular particles (Fig. 5a), with an overall Ca/P ratio (1.26 ± 0.04), (Table 4). After 30 days of storage in SBF crystals with rod-like morphology (Fig. 5b) could be detected. These latter newly-formed crystals had (Table 3) a Ca/P ratio quite different from that of the control HA (Table 4), but comparable to that of the calcium-deficient HA [43].

The experimental fluoride-doped VSG5F, VSG10F and VSG20F presented a FTIR spectrum comparable to that of the commercial hydroxyapatite used in this study. In accordance, the XRD analysis performed after 24 h of immersion in SBF showed the formation of apatite, with a residual presence of β-TCP and CaF_2 (Fig. 2A). After 15 d of

Table 4
Ca/P ratio of the tested materials after SBF storage.

	T0			1 month		
	Ca at%	P at%	**Ratio Ca/P (mol.)**	Ca at%	P at%	**Ratio Ca/P (mol.)**
HAp	50.7 ± 6.4	23.4 ± 2.8	**1.68 ± 0.15**	55.1 ± 5.6	25.2 ± 3.8	**1.70 ± 0.11**
VSG	23.3 ± 0.4	13.9 ± 0.4	**1.26 ± 0.04**	29.4 ± 6.8	17.1 ± 4.3	**1.34 ± 0.07**
VSG5F	31.5 ± 0.6	18.3 ± 0.3	**1.34 ± 0.05**	41.2 ± 3.8	18.9 ± 2.9	**1.68 ± 0.03**
VSG10F	31.6 ± 0.7	16.1 ± 0.6	**1.52 ± 0.09**	46.5 ± 5.1	21.2 ± 2.3	**1.69 ± 0.04**
VSG20F	32.3 ± 0.9	16.2 ± 0.9	**1.54 ± 0.05**	53.4 ± 6.2	23.7 ± 2.8	**1.74 ± 0.02**

immersion in SBF, the XRD results showed that VSG5F, VSG20F and VSG10F were characterised by the evident presence of HA, but still with residual presence of β-TCP (Fig. 2). However, these latter three fluoride-containing powders showed a greater relative intensity of the diffraction peaks (i.e., crystallinity, 2θ = 30.2∘(0 0 2)), indicating an excellent conversion into apatite after 30 d of SBF storage. Moreover, the peaks in the region of 30–35º became sharper as a consequence of enhanced crystallinity within the fluoride-doped VSG materials. The relativity intensity of the peak in 2θ = 32.3º (112) were greater than the peak in 2θ = 33.0º (030), so it possible to affirm that during SBF immersion the nanoparticles underwent a preferential orientation and resulting in a non-symmetric morphology transformation of the apatite crystals (Fig. 2C). Furthermore, the crystals size of the apatite calculated by means of XRD was very small in VSG even after 30 d in SBF (11.3 ± 0.3), while VSG10F and VSG20F showed a noticeable growth of the crystals both after 15 and 30 days of SBF immersion; VSG5F showed the smallest crystal size at all time periods (Table 3). However, it was interesting to note that VSG20 produced the largest crystals after 30 days of SBF storage compared to the other tested materials, and how such crystals increased in size with a magnitude of threefold compared to those observed at 24 h with the same material. We hypothesise that such results could be related to higher presence of fluoride ions released in the storage media (Table 1), which has favoured, along with calcium and phosphate ions, such an evident growth of the crystals up to that particular dimension.

Previous studies showed through XRD analysis that the crystallite size of apatite formed on bioactive glasses were in the range of 16–26 nm [49], while crystallites of FHA in fluoride-doped bioactive glasses could also reach a dimension of less than 50 nm [13]. Both the FIB-SEM (Fig. 4B) and TEM ultramorphology analysis confirmed that the VSG-F powders were able to form apatite-like crystals, with greater dimension and an evident rod-like morphology compared to the fluoride-free VSG (Fig. 5C and Table 3). The Ca/P ratio of the fluoride-doped CaP powders tested in this study was comparable to that of the HA after 30 days of storage in SBF (Table 4).

It is important to highlight that there was also an important formation of fluoride-based compounds (CaF_2), especially in VSG20F (Fig. 2C). As previously mentioned, the experimental fluoride-doped VSGs were formulated with different concentrations of calcium salts in order to trigger the formation of fluoride-containing apatite-like crystals. Hence, the first important aspect to discuss is the ability of the tested materials to release fluoride into the storage media (Table 1). It was observed that VSG5F had the lowest release of fluoride ions with no significant variation over time ($p > 0.05$) compared to the other fluoride-doped powders. Conversely, VSG10F showed important fluoride release, with the cumulative values that significantly increased over time. The experimental VSG20F presented the greatest (99.15 mg/L) release of fluoride with significant increase at day 1, day 30 and day ($p < 0.05$).

As mentioned in the introduction, the release of fluoride ions in saliva may prevent and/or arrest caries lesions thanks to the alteration of the metabolic activity of cariogenic bacterial in dental [10] or mineralisation of enamel through fluoride-containing apatite [9]. Indeed, it has been reported that fluoride ions can selectively substitute OH^- in HA and induce the formation of fluor-hydroxyapatite [FHA, $Ca_{10}(PO_4)6(OH_xF_y)$] [11,12]. However, it has been advocated that the formation of FHA may occur especially when there is the presence of relatively low concentration (< 45 ppm) of F^- ions, otherwise the main mineral phase to precipitate on the enamel surface would be CaF_2 [13,14]. In some ways, the results of the current study obtained during the 19F MAS NMR analysis confirmed that the lower the amount of fluoride incorporated into the experimental powers the greater the probability to form FHA, with less precipitation of CaF_2. Certainly, the NMR analysis performed on VSG5F and VSG10F after 30 d of immersion in SBF revealed the presence of fluorapatite-like phase and CaF_2; this latter was more evident in VSG20F. Conversely, VSG showed no presence of FHA or/and CaF_2 after 30 d of storage in SBF (Fig. 3).

It is well known that apatite deposition in SBF is clearly pH dependent, and that the rise of pH in SBF is less pronounced with increasing fluoride content in the fluoride-doped compounds such as bioactive glasses [50]. The results of the pH analysis performed in the current study (Table 1) are in agreement with those outcomes, so it might be one of the reasons why FHA was prioritised over HA deposition in our fluoride-doped VSGs. Hench et al. [51] showed that 45S5 bioactive glasses doped with fluoride were able to release fluoride ions and induce the formation of fluorite, which has a much lower solubility than HA and HCA at acidic pH (< 5.5). The results of the current study are in accordance with those reported in a recent study [52], where it was shown through ^{19}F MAS NMR how the presence of different concentrations of fluoride in sodium-free bioactive glasses could influence apatite deposition in SBF. Indeed, it was detected the presence of prominent peaks at − 102 ppm and − 107 ppm, which were assigned as an overlap between fluorapatite and fluorite. While, the broad signal between − 140 ppm to − 150 ppm may have arisen from the high content of Ca/Na fluorine that remained unreacted [13,52].

In the current study, the cytotoxicity of experimental fluoride-doped VSGs was also evaluated through MTT assay. Fluoride has been advocated to promote biological activities such as binding interactions, metabolic stability, and reduced toxicity at low concentrations [53,54]. According to this evidence, our results showed that the tested materials with greater toxicity on hDPSCs were the fluoride-free VSG (containing no fluoride) and VSG20F; this latter had the greatest release of fluoride ions when immersed in SBF (Table 2). Moreover, a rather similar trend was observed for all the specimens; a decrease in viability was detected when they were not diluted, with an increase in cell vitality for all powders at lower concentration (1:10, 1:50 and 1:100 dilutions) compared to the control. Such effects on cell proliferation could be explained by the possible presence of apatite and fluoride-containing apatite. Indeed, according to our data, the literature reports some evidence that the proliferation of human osteoblast-like (HO) cells increases by 10 % more in contact with fluoridated hydroxyapatite (FHA) compared to the control, but higher concentration of fluoride caused an impediment in the cell growth by about 2 days [54,55].

In view of the results obtained in this study, such fluoride-doped calcium-phosphates (VSG-F) might potentially be used as “bioactive” compounds into preventive products such as gels and toothpastes for remineralisation of enamel and dentine or incorporated as fillers in resin-based materials to generate adhesives and composites/cements able to protect and remineralise the dentine-material interface. Indeed,

our ongoing studies have been evaluating if their direct application on demineralised dentine may induce a proper intra-/extra-fibrillar collagen remineralisation. Moreover, we have already incorporated such experimental fluoride-doped calcium phosphates in resin-based materials to evaluate their ability in remineralising the bonding interface created in caries-affected dentine.

5. Conclusions

The experimental calcium phosphates tailored with different concentrations of fluoride salts have the ability to convert into biocompatible fluoride-containing apatite-like crystals when immersed in SBF for 30 d, especially those with lower concentration of fluoride salts (5 wt% and 10 wt%). Hence, within the limitation of this study, such experimental materials might be considered as promising remineralising resources for dental applications.

Acknowledgements

All authors gave their final approval and agree to be accountable for all aspects of the work. There is a patent on the calcium phosphates tailored with different concentrations of fluoride salts used in this study (ES2716942 - Composicion Y Procedimiento Para La Obtencion Y Aplicacion De Un Compuesto Bioactivo Que Contiene Fluoruro Y El Producto Obtenido). The authors have no financial affiliation or involvement with any commercial organization with direct financial interest in the materials discussed in this manuscript. This study was supported by grants “Ministerio de Ciencia, Innovación y Universidades (PID2020–120346 GB-I00) and the authors acknowledge the use of the Department of Chemistry NMR Facility at the University of Manchester. This study was also supported in part by the Coordenação de Aperfeiçoamento de Pessoal de Nível Superior (CAPES-Brazil) – Finance Code AUXPE 23038.006958/2014–96 (PI VPF). The authors are grateful to X-ray Laboratory of Federal University of Ceara for XRD measurements.

References

[1] Banerjee A, Frencken JE, Schwendicke F, Innes NPT. Contemporary operative caries management: consensus recommendations on minimally invasive caries removal. Br Dent J 2017;223(3):215–22. https://doi.org/10.1038/sj.bdj.2017.672
[2] Frencken JE, Peters MC, Manton DJ, Leal SC, Gordan VV, Eden E. Minimal intervention dentistry for managing dental caries - a review: report of a FDI task group. Int Dent J 2012;62(5):223–43. https://doi.org/10.1111/idj.12007
[3] Abou Neel EA, Aljabo A, Strange A, Ibrahim S, Coathup M, Young AM, Bozec L, Mudera V. Demineralization-remineralization dynamics in teeth and bone. Int J Nanomedicine 2016;19(11):4743–63. https://doi.org/10.2147/IJN.S107624
[4] Cochrane NJ, Cai F, Huq NL, Burrow MF, Reynolds EC. New approaches to enhanced remineralization of tooth enamel. J Dent Res 2010;89(11):1187–97. https://doi.org/10.1177/0022034510376046
[5] Fernando JR, Shen P, Walker GD, Yuan Y, Stanton DP, Reynolds C, et al. Acceleration of enamel subsurface lesion remineralisation by intralesion pH modulation. Caries Res 2021;55(2):130–6. https://doi.org/10.1159/000513609
[6] Bashir E, Lagerlöf F. Effect of citric acid clearance on the saturation with respect to hydroxyapatite in saliva. Caries Res 1996;30(3):213–7. https://doi.org/10.1159/000262162
[7] Zhang X, Deng X, Wu Y. Kishen Anil, editor. Nanotechnology in Endodontics: Current and Potential Clinical Applications. Springer International Publishing; 2015. p. 173–93.
[8] Zero DT. Dentifrices, mouthwashes, and remineralization/caries arrestment strategies. BMC Oral Health 2006;15(6). https://doi.org/10.1186/1472-6831-6-S1-S9. Suppl 1(Suppl 1):S9.
[9] ten Cate JM. Contemporary perspective on the use of fluoride products in caries prevention. Br Dent J 2013;214(4):161–7. https://doi.org/10.1038/sj.bdj.2013.162
[10] Lynch RJ, Navada R, Walia R. Low-levels of fluoride in plaque and saliva and their effects on the demineralisation and remineralisation of enamel; role of fluoride toothpastes. Int Dent J 2004;54(5 Suppl 1):304–9. https://doi.org/10.1111/j.1875-595x.2004.tb00003.x
[11] Brauer DS, Karpukhina N, O'Donnell MD, Law RV, Hill RG. Fluoride-containing bioactive glasses: effect of glass design and structure on degradation, pH and apatite formation in simulated body fluid. Acta Biomater 2010;6(8):3275–82. https://doi.org/10.1016/j.actbio.2010.01.043
[12] Mohammed NR, Kent NW, Lynch RJ, Karpukhina N, Hill R, Anderson P. Effects of fluoride on in vitro enamel demineralisation analyzed by ^{19}F MAS NMR. Caries Res 2013;47(5):421–8. https://doi.org/10.1159/000350171
[13] Kim HW, Kim HE, Knowles JC. Fluor-hydroxyapatite sol-gel coating on titanium substrate for hard tissue implants. Biomaterials 2004;25(17):3351–8. https://doi.org/10.1016/j.biomaterials.2003.09.104
[14] Tredwin CJ, Young AM, Abou Neel EA, Georgiou G, Knowles JC. Hydroxyapatite, fluor-hydroxyapatite and fluorapatite produced via the sol-gel method: dissolution behaviour and biological properties after crystallisation. J Mater Sci Mater Med 2014;25(1):47–53. https://doi.org/10.1007/s10856-013-5050-y
[15] Zhao J, Liu Y, Sun WB, Zhang H. Amorphous calcium phosphate and its application in dentistry. Chem Cent J 2011;5(40). https://doi.org/10.1186/1752-153X-5-40
[16] Viana ÍEL, Lopes RM, Silva FRO, Lima NB, Aranha ACC, Feitosa S, et al. Novel fluoride and stannous -functionalized β-tricalcium phosphate nanoparticles for the management of dental erosion. J Dent 2020;92:103263. https://doi.org/10.1016/j.jdent.2019.103263
[17] Angelini Sfalcin R, da Silva JVP, Oliva Pessoa V, Santos J, Garcia Olivan SR, Porta Santos Fernandes K, et al. Remineralisation of early enamel caries lesions induced by bioactive particles: an in vitro speckle analysis. Photo Photo Ther 2019;28:201–9. https://doi.org/10.1016/j.pdpdt.2019.07.022
[18] Ramadoss R, Padmanaban R, Subramanian B. Role of bioglass in enamel remineralisation: existing strategies and future prospects – a narrative review. J Biomed Mater Res B Appl Biomater 2022;110(1):45–66. https://doi.org/10.1002/jbm.b.34904
[19] Sauro S, Babbar A, Gharibi B, Feitosa VP, Carvalho RM, Azevedo Rodrigues LK, et al. Cellular differentiation, bioactive and mechanical properties of experimental light-curing pulp protection materials. Dent Mater 2018;34(6):868–78. https://doi.org/10.1016/j.dental.2018.02.008
[20] Sauro S, Osorio R, Fulgêncio R, Watson TF, Cama G, Thompson I, et al. Remineralisation properties of innovative light-curable resin-based dental materials containing bioactive micro-fillers. J Mater Chem B 2013;1(20):2624–38. https://doi.org/10.1039/c3tb00205e
[21] Tay FR, Pashley DH. Biomimetic remineralization of resin-bonded acid-etched dentin. J Dent Res 2009;88(8):719–24. https://doi.org/10.1177/0022034509341826
[22] Osorio R, Yamauti M, Sauro S, Watson TF, Toledano M. Zinc incorporation improves biological activity of beta-tricalcium silicate resin-based cement. J Endod 2014;40(11):1840–5. https://doi.org/10.1016/j.joen.2014.06.016
[23] Profeta AC, Mannocci F, Foxton R, Watson TF, Feitosa VP, De Carlo B, et al. Experimental etch-and-rinse adhesives doped with bioactive calcium silicate-based micro-fillers to generate therapeutic resin-dentin interfaces. Dent Mater 2013;29(7):729–41. https://doi.org/10.1016/j.dental.2013.04.001
[24] Sauro S, Osorio R, Watson TF, Toledano M. Influence of phosphoproteins' biomimetic analogs on remineralization of mineral-depleted resin-dentin interfaces created with ion-releasing resin-based systems. Dent Mater 2015;31(7):759–77. https://doi.org/10.1016/j.dental.2015.03.013
[25] Gu LS, Kim J, Kim YK, Liu Y, Dickens SH, Pashley DH, et al. A chemical phosphorylation-inspired design for Type I collagen biomimetic remineralization. Dent Mater 2010;26(11):1077–89. https://doi.org/10.1016/j.dental.2010.07.008
[26] Niu LN, Zhang W, Pashley DH, Breschi L, Mao J, Chen JH, et al. Biomimetic remineralization of dentin. Dent Mater 2014;30(1):77–96. https://doi.org/10.1016/j.dental.2013.07.013
[27] Tezvergil-Mutluay A, Seseogullari-Dirihan R, Feitosa VP, Tay FR, Watson TF, Pashley DH, et al. Zoledronate and ion-releasing resins impair dentin collagen degradation. J Dent Res 2014;93(10):999–1004. https://doi.org/10.1177/0022034514546043
[28] Imazato S. Antibacterial properties of resin composites and dentin bonding systems. Dent Mater 2003;19(6):449–57. https://doi.org/10.1016/s0109-5641(02)00102-1
[29] Khvostenko D, Hilton TJ, Ferracane JL, Mitchell JC, Kruzic JJ. Bioactive glass fillers reduce bacterial penetration into marginal gaps for composite restorations. Dent Mater 2016;32(1):73–81. https://doi.org/10.1016/j.dental.2015.10.007
[30] Aponso S, Ummadi JG, Davis H, Ferracane J, Koley D. A chemical approach to optimizing bioactive glass dental composites. J Dent Res 2019;98(2):194–9. https://doi.org/10.1177/0022034518809086
[31] Sauro S, Feitosa VP. Preparation, Composition and Application of a Bioactive Fluoride-Doped Calcium Phosphate Able to Induce Controlled Deposition of Fluorapatite. W.O. Patent No 2019/243592 A1. Geneva: World Intellectual Property Organization,; 2019.
[32] Kokubo T, Kushitani H, Sakka S, Kitsugi T, Yamamuro T. Solutions able to reproduce in vivo surface-structure changes in bioactive glass-ceramic A-W. J Biomed Mater Res 1990;24(6):721–34. https://doi.org/10.1002/jbm.820240607
[33] Bleicher L, Sasaki JM, et al. Development of graphical interface for the Rietveld refinement program DBWS. J Appl Crystallogr 2000;v. 33.
[34] Freire RM, Ribeiro TS, Vasconcelos IF, et al. $MZnFe_2O_4$ (M = Ni, Mn) cubic superparamagnetic nanoparticles obtained by hydrothermal synthesis. J Nanopart Res 2013;15:1616. https://doi.org/10.1007/s11051-013-1616-3
[35] Hill RJ, Howard CJ. Quantitative phase analysis from neutron powder diffraction data using the Rietveld method. J. Appl. Cryst 1987;20:467–74. https://doi.org/10.1107/S0021889887086199
[36] Takadama H, Kim HM, Kokubo T, Nakamura T. TEM-EDX study of mechanism of bonelike apatite formation on bioactive titanium metal in simulated body fluid. J Biomed Mater Res 2001;57(3):441–8. https://doi.org/10.1002/1097-4636(20011205)57:3<441::aid-jbm1187>3.0.co;2-b
[37] ISO 10993–12. Biological evaluation of medical devices. Part 12: sample preparation and reference materials; 2009.
[38] Spagnuolo G, Pires PM, Calarco A, Peluso G, Banerjee A, Rengo S, et al. An in-vitro study investigating the effect of air-abrasion bioactive glasses on dental adhesion, cytotoxicity and odontogenic gene expression. Dent Mater 2021;37(11):1734–50. https://doi.org/10.1016/j.dental.2021.09.004

[39] Andrade Neto DM, Carvalho EV, Rodrigues EA, Feitosa VP, Sauro S, Mele G, et al. Novel hydroxyapatite nanorods improve anti-caries efficacy of enamel infiltrants. Dent Mater 2016;32(6):784–93. https://doi.org/10.1016/j.dental.2016.03.026
[40] LeGeros RZ, Sakae T, Bautista C, Retino M, LeGeros JP. Magnesium and carbonate in enamel and synthetic apatites. Adv Dent Res 1996;10(2):225–31. https://doi.org/10.1177/08959374960100021801
[41] Tavares Ddos S, Castro Lde O, Soares GD, Alves GG, Granjeiro JM. Synthesis and cytotoxicity evaluation of granular magnesium substituted β-tricalcium phosphate. J Appl Oral Sci 2013;21(1):37–42. https://doi.org/10.1590/1678-7757201302138
[42] Tredwin CJ, Georgiou G, Kim H-W, Knowles JC. Hydroxyapatite, fluor-hydroxyapatite and fluorapatite produced via the sol–gel method: Bonding to titanium and scanning electron microscopy. Dent Mater 2013;29:521. https://doi.org/10.1016/j.dental.2013.02.002
[43] Dorozhkin SV. Calcium orthophosphates (CaPO4): occurrence and properties. Prog Biomater 2016;5:9–70.
[44] Sauro S, Lin CY, Bikker FJ, Cama G, Dubruel P, Soria JM, et al. Di-calcium phosphate and phytosphingosine as an innovative acid-resistant treatment to occlude dentine tubules. Caries Res 2016;50(3):303–9. https://doi.org/10.1159/000445444
[45] Cama G, Barberis F, Botter R, Cirillo P, Capurro M, Quarto R, et al. Preparation and properties of macroporous brushite bone cements. Acta Biomater 2009;5(6):2161–8. https://doi.org/10.1016/j.actbio.2009.02.012
[46] Jiang W, Chu X, Wang B, Pan H, Xu X, Tang R. Biomimetically triggered inorganic crystal transformation by biomolecules: a new understanding of biomineralization. J Phys Chem B 2009;113(31):10838–44. https://doi.org/10.1021/jp904633f
[47] Takagi S, Chow LC, Ishikawa K. Formation of hydroxyapatite in new calcium phosphate cements. Biomaterials 1998;19(17):1593–9. https://doi.org/10.1016/s0142-9612(97)00119-1
[48] Vijayalakshmi Sanyal M, Rajendran C, Ramachandra Raja C. Effect of calcium carbonate in the studies and synthesis of hydroxyapatite. Adv Mater Res 2012;584:450–4. https://doi.org/10.4028/www.scientific.net/AMR.584.450
[49] O'Donnell MD, Watts SJ, Hill RG, Law RV. The effect of phosphate content on the bioactivity of soda-lime-phosphosilicate glasses. J Mater Sci-Mater Med 2009;20:1611–8.
[50] Lu X, Leng Y. Theoretical analysis of calcium phosphate precipitation in simulated body fluid. Biomaterials 2005;26(10):1097–108. https://doi.org/10.1016/j.biomaterials.2004.05.034
[51] Hench L.L., Spilman D.B., Hench J.W., inventors; University of Florida, assignee. Fluoride-modified bioactive glass (Bioglass) and its use as implant material. US patent 4775646; 1988.
[52] Shaharyar Y, Wein E, Kim JJ, Youngman RE, Muñoz F, Kim HW, et al. Structure-solubility relationships in fluoride-containing phosphate based bioactive glasses. J Mater Chem B 2015;3(48):9360–73. https://doi.org/10.1039/c5tb01494h
[53] Hagmann WK. The many roles for fluorine in medicinal chemistry. J Med Chem 2008;51(15):4359–69. https://doi.org/10.1021/jm800219f
[54] Kyzer JL, Martens M. Metabolism and toxicity of fluorine compounds. Chem Res Toxicol 2021;34(3):678–80. https://doi.org/10.1021/acs.chemrestox.0c00439
[55] Esnaashary M, Fathi M, Ahmadian M. In vitro evaluation of human osteoblast-like cell proliferation and attachment on nanostructured fluoridated hydroxyapatite. Biotechnol Lett 2014;36(6):1343–7. https://doi.org/10.1007/s10529-014-1483-8